AIP | Applied Physics Letters

Surface double-layer structure in (110) oriented BiFeO3 thin film

Tieying Yang, Can Wang, Xingmin Zhang, Yu Feng, Haizhong Guo, Kuijuan Jin, Xingyu Gao, Zhong Li, and Xiaolong Li

Citation: Applied Physics Letters **105**, 202901 (2014); doi: 10.1063/1.4902113
View online: http://dx.doi.org/10.1063/1.4902113
View Table of Contents: http://scitation.aip.org/content/aip/journal/apl/105/20?ver=pdfcov
Published by the AIP Publishing

Surface double-layer structure in (110) oriented $BiFeO_3$ thin film

Tieying Yang,[1] Can Wang,[2] Xingmin Zhang,[1] Yu Feng,[2] Haizhong Guo,[2] Kuijuan Jin,[2] Xingyu Gao,[1] Zhong Li,[1] and Xiaolong Li[1,a)]
[1]*Shanghai Institute of Applied Physics, Chinese Academy of Sciences, Shanghai 201204, China*
[2]*Institute of Physics, Chinese Academy of Sciences, Beijing 100190, China*

(Received 24 September 2014; accepted 7 November 2014; published online 17 November 2014)

Surface double-layer structure different from the interior was found in $BiFeO_3$ thin film grown on $SrRuO_3$ covered $SrTiO_3$ (110) substrate by pulsed laser deposition. It was shown that $BiFeO_3$ film exhibits epitaxial phase with single domain. X-ray reflectivity and X-ray photoelectron spectroscopy results revealed a skin layer of less than 1 nm with a reduced electron density and different surface state. Grazing incidence x-ray diffraction convinced a surface multi-domain structure of several nm beneath the surface skin layer. The double-layer near surface structure would be originated from the large depolarization field produced by the single-domain structure with strain.
 [http://dx.doi.org/10.1063/1.4902113]

$BiFeO_3$ (BFO) is one of the most important multiferroic oxides with high ferroelectric, ferromagnetic ordering temperature, and large ferroelectric polarization.[1] Owing to its intriguing properties, BFO has the potential to be used in next generation devices such as information storage, spintronics, and sensors.[2–4] All these applications are realized in complex components or thin-film geometries. In this case, the surface of ferroelectric can significantly affect the multiferroic properties.[5] Therefore, it is important to understand and control the surface structure of ferroelectrics. Actually, ferroelectric surface has been widely studied, it is well known that structural or electronic surface layers exist at the surface of $SrTiO_3$ (STO), $BaTiO_3$, and $PbTiO_3$.[6–9] However, the near surface structure of BFO remains not very clear and needs better understanding.

Recent studies have reported surface layer also exists at BFO single crystal,[10] the skin layer of several nm has different lattice parameters and Bi core level state different from those of the bulk. Further investigation suggests that there should be two layers at the surface of BFO single crystal, a ferroelectrically "dead" outer skin and a subsurface nanodomains layer of less than a micron deep.[11] However, up to now, most of the research on BFO surface has been performed on single crystal, very little attention has been paid to the surface of BFO films. Due to the variety of strain, orientation, interface, and size effect, the surface of ferroelectric films can be rather complex than that of single crystal.[12] In this work, we investigate the surface structure of epitaxial BFO film on $SrTiO_3$ (110) substrate by X-ray reflectivity (XRR), X-ray diffraction, angle-resolved X-ray photoelectron spectroscopy (XPS), and Grazing incidence X-ray diffraction (GID). We found that there are two layers at the surface of BFO film: a skin layer of less than 1 nm with reduced electron density and different surface state and a surface multi-domain structure of several nm beneath the skin layer.

The BFO film was deposited on single crystal STO (110) substrate with $SrRuO_3$ (SRO) bottom electric layer by the pulsed laser deposition (PLD) equipped with reflection high-energy electron diffraction (RHEED). The substrate temperature was maintained at 610 °C and the oxygen partial pressure was kept at 10 Pa during the deposition process. The thickness of BFO film used in this study is about 300 nm. The detailed deposition conditions have been described elsewhere.[13] The microstructure was characterized at beamline BL14B1 of Shanghai Synchrotron Radiation Facility (SSRF) with a wavelength of 1.2387 Å. XPS measurements were performed using an Al Kα radiation (1486.6 eV) at 3×10^{-9} mbar background pressure.

X-ray diffraction results (theta-2theta, phi scan, not shown) reveal that the film is composed of phase-pure, epitaxial BFO and SRO on STO substrate aligned along the (110) direction. Fig. 1(a) shows the reciprocal space mapping (RSM) figure around the (110) reflection of STO, the lattice constant was calculated using the angular position of the Bragg reflection. From the measurement, we determine that the interplanar spacing of BFO pseudocubic (110) is about 2.83 Å, which is slightly larger than that of bulk phase (2.80 Å).[14] The elongation of d (110) is a result of the in-plane compression from STO substrate. The in-plane structure of the film was examined by an asymmetric RSM scan around the (221) plane of STO (Fig. 1(b)). From the RSM figure, we found that BFO Bragg peak is located outside of the vertically line, indicating that the epitaxial strain from substrate has been partly relaxed. The elongate of the peak in Q_x direction would reflect the strain relaxation process along the growth direction. Furthermore, we found that BFO peaks do not exhibit any splitting of the (110) and (221) reflections, indicating a single domain structure of BFO. The formation of the single domain state might be due to the small miscut angle of the substrate.[15]

Fig. 2 shows the XRR profile of the sample measured in air. To present the interference fringes more clearly, we also plotted the reflectivity data as $R*Q_z^4$ vs Q_z in Fig. 2, where $Q_z = 4\pi \sin\theta/\lambda$ is the vertical wave-vector transfer. A broad bump can be seen between 0.2 and 0.25 $Å^{-1}$, indicating that a surface structure is present on top of the film with an electron density different from the underlying BFO layer. We simulated the XRR profile using the matrix formalism corrected by a Croce–Nevot factor.[16,17] However, we found that

a)E-mail: lixiaolong@sinap.ac.cn. Tel./Fax: 86-021-33933215.

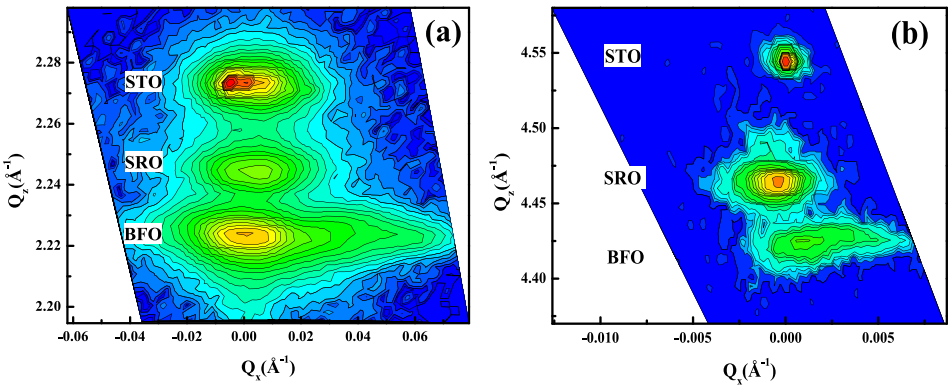

FIG. 1. X-ray RSMs around (110) reflection (a) and asymmetric (221) reflection of STO (b).

the model including only one surface layer fails to reproduce the experimental data with reasonable parameters, an additional skin layer has to be added to obtain better fitting. The electron density profile obtained from the fitting data is shown in the inset of Fig. 2; one finds clearly that there are three regions in the curve, corresponding to the BFO layer, the surface layer, and the skin layer. The BFO layer has an electron density of 2.06 $e^-/Å^3$, this value is very close to the electron density of bulk BFO phase (about 2.13 $e^-/Å^3$), indicating that the film has a dense structure. The surface layer has a thickness of about 3 nm with an electron density of 1.99 $e^-/Å^3$, which is slightly smaller than that of the beneath BFO layer. The skin layer has a smallest electron density with a thickness of about 8 Å, related to the surface relaxation of BFO in the surface region. Atomic force microscopy (AFM) was used to probe the surface morphology; we found that local RMS (root mean square) roughness of the surface is about 1.03 Å. This value is almost equal to the thickness of the skin layer obtained from the fitting. According to the AFM results, the XRR simulation is considered to be reasonable. To further verify this two-layer model, we performed XPS and GID experiments, respectively.

Angle resolved XPS can provide chemical state and depth distribution of elements at the near surface region. Fig. 3 shows the Bi 4f core-level spectra of the sample taken at the takeoff angle of 20° (surface sensitive), 60°, and 90° (bulk sensitive), respectively. Two components are observed in the Bi 4f spectra indicating two different electronic environments. Moreover, with the decreasing of the takeoff angle, the intensity of the higher binding energy component increases, indicating that this component is originated from the surface (Bi surface state). The thickness of the layer containing Bi surface state can be estimated by the formula $d = \lambda \sin\alpha \times \ln(R/R_\infty + 1)$,[18] where λ is the mean attenuation length (about 20.1 Å),[19] α is the takeoff angle, R is the intensity ratio of $I_{surface}/I_{bulk}$, and R_∞ is the ratio $I_{surface}/I_{bulk}$ in the case of infinitely thick surface layer and bulk sample (approximately to be 1). The plot of $\ln(R/R_\infty + 1)$ versus $1/\sin\alpha$ will produce a straight line through zero whose slope is d/λ, and therefore, we obtain the thickness of the layer contained Bi surface state, to be about 3.5 Å. This value is slightly smaller than that of the skin layer (about 8 Å) from XRR simulation, which suggests that the Bi surface state should be originated from the low electron density skin layer.

To obtain the surface structure of BFO, we perform GID experiments on the sample in both in-plane directions. Depth-dependence structure information can be obtained by this technique, as the incident angle of x-ray beam is less than critical angle, the penetration depth of the x-rays becomes on the nanometer order. The critical angle of BFO is calculated to be about 0.31° at 10 keV, corresponding to a penetration depth of about 5 nm. The in-plane interplanar spacings, as determined from the (002) and (1–1 0) diffraction peaks at different incident angles, are plotted in Fig. 4(a). When the incident angle is larger than 0.35°, the interplanar spacings of both in-plane axis almost keep constant. However, when the incident angle is smaller than 0.35°, it is impressive to find

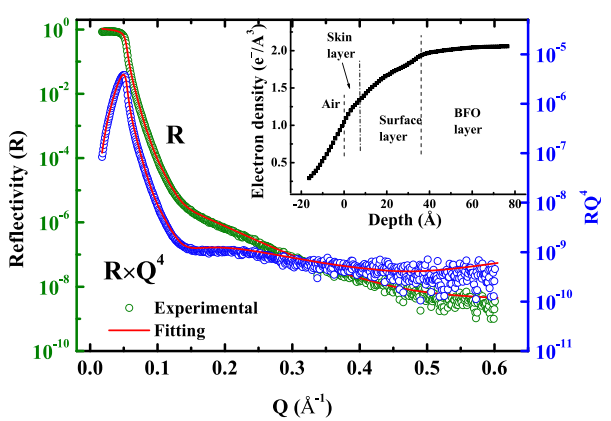

FIG. 2. X-ray reflectivity profiles of the sample, $R \times q_z^4$ VS q_z to enhance the oscillations. Inset: electron density profile derived from the reflectivity data.

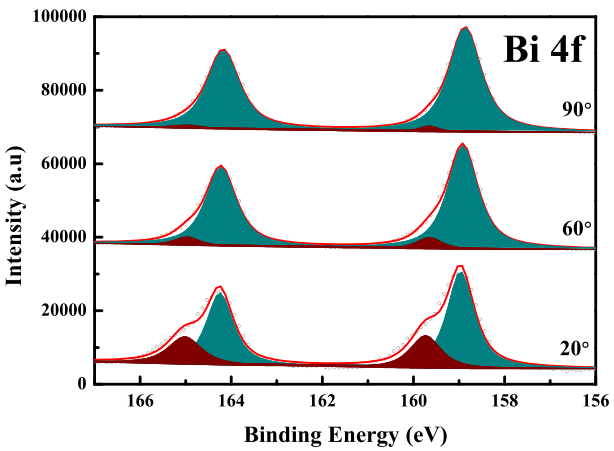

FIG. 3. Angle-resolved XPS spectra of Bi 4f core-level taken at the takeoff angle of 20° (surface sensitive), 60°, 90° (bulk sensitive), respectively.

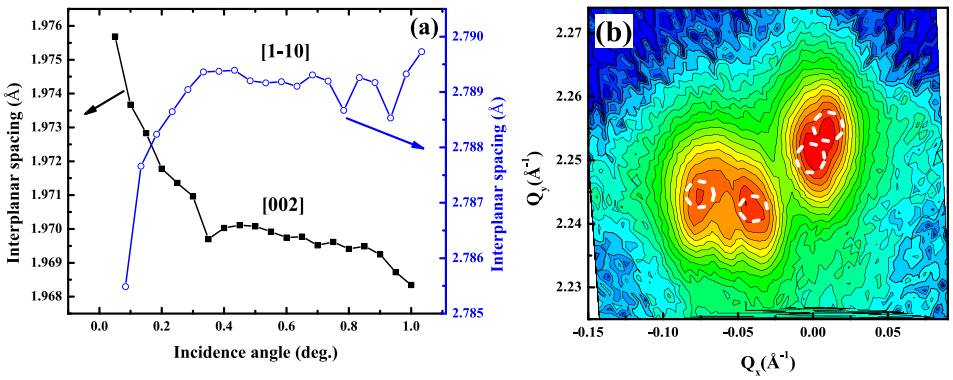

FIG. 4. (a) The variation of in-plane (002) and (1-1 0) lattices with incidence angle. (b) In-plane RSM around (1–10) reflection of BFO at incident angle of 0.2°.

that the interplanar spacing of (002) increases from 1.969 Å to 1.976 Å, meanwhile, that of (1–10) decreases from 2.789 Å to 2.786 Å. From these results, we conclude that the surface region (estimated to be about 5 nm) should have different structure with the interior of the film, consistent with the surface layer in XRR model. The different variation tendency of *d* (002) and *d* (1–10) in the surface layer should imply a complex strain relaxation mechanism in the film, which might lead to a different phase or domain structure in the near surface region.[20,21] In order to clarify this, RSM analysis was performed under grazing incidence condition. Fig. 4(b) shows the in-plane RSM figure around (1–10) peak of STO at incident angle of 0.2°, it can be seen that four peaks (marked with white circle) exist in the RSM. Since the (1–10) reflection is sensitive to the structural difference between BFO ferroelectric domains, the existence of four (1–10) structure variants indicate that the surface layer should encompass four polarization directions.[22,23] In other words, the surface layer of several nm presents multi-domain structure.

Based on the above analysis, the double-layer surface structure of BFO by XRR fitting has been proved to be reasonable. There are two layers on top of the (110) oriented BFO film, a surface relaxation layer of less than 1 nm, and a surface multi-domain layer of about several nm. These results are different with that of BFO single crystals, which reported a skin layer about several nm or surface domain structure of about a micron,[10,11] the reason might be due to the different surface effect and strain state between films with bulk. Our results are also different with the BFO films on $LaAlO_3$ (LAO) substrates.[24,25] Infante *et al*. investigated the structure of BFO film and revealed a T-like phase due to the large misfit strain of about −4.8% between BFO and LAO,[24] the strain is released by the coexistence phases of T-like and R-like. In our study, the strain from STO substrate is partly released by the formation of single domain and complex surface structure. This might be the result of the smaller lattice misfit of −1.3% between BFO and STO, which convinced that strains will significantly affect the structure of ferroelectric films.

Due to the ferroelectric polarization, a lot of macroscopic electric charges gather at the surface of ferroelectrics, the unshielded surface charges can generate a large depolarization field, which is considered to be a dominant controlling factor of the surface effect in ferroelectrics. This field can be screened by a variety of mechanisms, such as surface free charge, surface relaxation, dead layer, or surface ordered domains, depending on various ferroelectrics or electrical boundary conditions.[26]

In fact, the surface structure of the ferroelectric films can be rather complex due to variety of strain and growth processing conditions.[27] Our results convince that single-domain ferroelectric state cannot be stabilized in the (110) oriented BFO film. Meanwhile, the top unit-cell suffers different chemical environment due to surface termination, which produces a different electric structure with relaxed lattice, thereby compensate the depolarization field to reach a more stable surface state.

In summary, the surface of epitaxial BFO/SRO/STO film was investigated in this work. It was shown that two layers exist at the surface of BFO film: a skin layer of less than 1 nm with reduced electron density and different surface state on top of the film, and a surface layer of several nm with multi-domain structure beneath the skin layer. The double-layer near surface structure would be originated from the large depolarization field produced by the single-domain structure.

The authors would like to thank the staff at beamline BL14B1 of Shanghai Synchrotron Radiation Facility. This work was financially supported by the National Natural Science Foundation of China (Nos. 11205235, 11405253, 11174355, and U1332205), the National Basic Research Program of China (Nos. 2010CB934501 and 2014CB921002), and the Knowledge Innovation Program of Chinese Academy of Sciences.

[1]N. A. Spaldin and M. Fiebig, Science **309**, 391 (2005).
[2]J. Wang, J. B. Neaton, H. Zheng, V. Nagarajan, S. B. Ogale, B. Liu, D. Viehland, V. Vaithyanathan, D. G. Schlom, U. V. Waghmare *et al*., Science **299**, 1719 (2003).
[3]T.-J. Park, G. C. Papaefthymiou, A. J. Viescas, A. R. Moodenbaugh, and S. S. Wong, Nano Lett. **7**, 766 (2007).
[4]G. Catalan and J. F. Scott, Adv. Mater. **21**, 2463 (2009).
[5]D. G. Schlom, L.-Q. Chen, C.-B. Eom, K. M. Rabe, S. K. Streiffer, and J.-M. Triscone, Annu. Rev. Mater. Res. **37**, 589 (2007).
[6]J. L. Wang, B. Vilquin, and N. Barrett, Appl. Phys. Lett. **101**, 092902 (2012).
[7]X. L. Li, H. B. Lu, M. Li, Z. Mai, H. Kim, and Q. J. Jia, Appl. Phys. Lett. **92**, 012902 (2008).
[8]S. Ravy, D. Le Bolloc'h, R. Currat, A. Fluerasu, C. Mocuta, and B. Dkhil, Phys. Rev. Lett. **98**, 105501 (2007).
[9]M. Sepliarsky, M. Stachiotti, and R. Migoni, Phys. Rev. Lett. **96**, 137603 (2006).
[10]X. Mart, P. Ferrer, J. Herrero-Albillos, J. Narvaez, V. Holy, N. Barrett, M. Alexe, and G. Catalan, Phys. Rev. Lett. **106**, 236101 (2011).
[11]N. Domingo, J. Narvaez, M. Alexe, and G. Catalan, J. Appl. Phys. **113**, 187220 (2013).

[12]D. Li, M. H. Zhao, J. Garra, A. M. Kolpak, A. M. Rappe, D. A. Bonnell, and J. M. Vohs, Nat. Mater. **7**, 473 (2008).
[13]C. Wang, K.-j. Jin, Z.-t. Xu, L. Wang, C. Ge, H.-b. Lu, H.-z. Guo, M. He, and G.-z. Yang, Appl. Phys. Lett. **98**, 192901 (2011).
[14]F. Kubel and H. Schmid, "Structure of a ferroelectric and ferroelastic monodomain crystal of the perovskite $BiFeO_3$," Acta Crystallogr., Sect. B. **46**, 698 (1990).
[15]C. J. M. Daumont, S. Farokhipoor, A. Ferri, J. C. Wojdeł, J. Íñiguez, B. J. Kooi, and B. Noheda, Phys. Rev. B **81**, 144115 (2010).
[16]C. Wiemer, S. Ferrari, M. Fanciulli, G. Pavia, and L. Lutterotti, Thin Solid Films **450**, 134 (2004).
[17]*X-ray and Neutron Reflectivity: Principles and Applications*, edited by J. Daillant and A. Gibaud (Springer, Berlin, 1999).
[18]*Practical Surface Analysis: Auger and X-ray Photoelectron Spectroscopy*, edited by D. Briggs and M. P. Seah (Wiley, Chichester, 1990), Vol. 1.
[19]C. J. Powell and A. Jablonski, NIST Electron Effective-Attenuation-Length Database, SRD 82, Version 1.1, National Institute of Standards and Technology, Gaithersburg, 2003.
[20]H. Liu, P. Yang, Z. Fan, A. Kumar, K. Yao, K. P. Ong, K. Zeng, and J. Wang, Phys. Rev. B **87**, 220101 (2013).
[21]M. Ramazanoglu, W. Ratcliff II, H. T. Yi, A. A. Sirenko, S. W. Cheong, and V. Kiryukhin, Phys. Rev. Lett. **107**, 067203 (2011).
[22]C. Huang, L. Chen, J. Wang, Q. He, S. Yang, Y. Chu, and R. Ramesh, Phys. Rev. B **80**, 140101(R) (2009).
[23]Y. H. Chu, M. P. Cruz, C. H. Yang, L. W. Martin, P. L. Yang, J. X. Zhang, K. Lee, P. Yu, L. Q. Chen, and R. Ramesh, Adv. Mater. **19**, 2662 (2007).
[24]I. C. Infante, J. Juraszek, S. Fusil, B. Dupé, P. Gemeiner, O. Diéguez, F. Pailloux, S. Jouen, E. Jacquet, G. Geneste *et al.*, Phys. Rev. Lett. **107**, 237601(2011).
[25]H. Béa, B. Dupé, S. Fusil, R. Mattana, E. Jacquet, B. Warot-Fonrose, F. Wilhelm, A. Rogalev, S. Petit, V. Cros *et al.*, Phys. Rev. Lett. **102**, 217603 (2009).
[26]J. Junquera and Ph. Ghosez, Nature **422**, 506 (2003).
[27]D. D. Fong, G. B. Stephenson, S. K. Streiffer, J. A. Eastman, O. Auciello, P. H. Fuoss, and C. Thompson, Science **304**, 1650 (2004).